Journal of Colloid and Interface Science 652 (2023) 2054–2065

Contents lists available at ScienceDirect

Journal of Colloid And Interface Science

journal homepage: www.elsevier.com/locate/jcis

Preparation of acid-responsive antibubbles from $CaCO_3$-based Pickering emulsions

Rabia Zia [a], Albert T. Poortinga [b], Akmal Nazir [c,*], Mutamed Ayyash [c], Cornelus F. van Nostrum [a,*]

[a] Department of Pharmaceutics, Utrecht Institute for Pharmaceutical Sciences, Utrecht University, Utrecht, the Netherlands
[b] Department of Mechanical Engineering, Polymer Technology, Eindhoven University of Technology, Eindhoven, the Netherlands
[c] Department of Food Science, College of Agriculture and Veterinary Medicine, United Arab Emirates University, Al Ain, United Arab Emirates

GRAPHICAL ABSTRACT

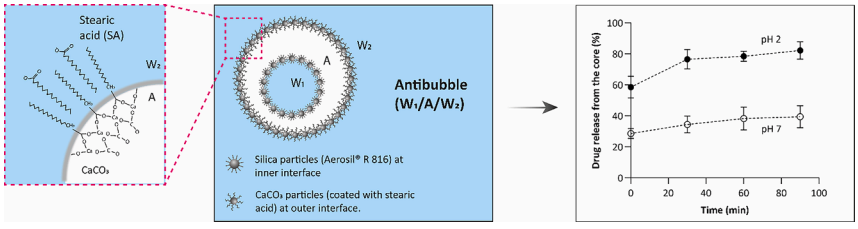

ARTICLE INFO

Keywords:
Antibubble
Pickering emulsion
$CaCO_3$
Acid-responsive
Drug delivery

ABSTRACT

Hypothesis: Hydrophobized fumed silica particles were previously reported for producing antibubbles that are quite stable in neutral as well as in acidic media. To produce acid-responsive antibubbles (e.g., for gastric drug delivery), the silica nanoparticles must be replaced by suitable particles, e.g., calcium carbonate ($CaCO_3$), which can degrade at low pH to release the encapsulated drug.

Experiments: Two variants of $CaCO_3$-stabilized antibubbles were prepared (by using $CaCO_3$ particles pre-coated with stearic acid, or by using native $CaCO_3$ particles in combination with sodium stearoyl lactylate) and drug release was compared with classic antibubbles produced with hydrophobized fumed silica particles.

Findings: $CaCO_3$ particles (pre-coated with stearic acid) can be used to produce stable antibubbles, which provided an entrapment efficiency of a model drug (methylene blue, MB) of around 85%. A burst release of MB (~60%) from the antibubbles was observed at pH 2 (i.e., the pH of the stomach), which was further increased to 80% during the next 30 min. On the contrary, at neutral pH, about 70% of the drug remained encapsulated for at least 2 h. We further demonstrated that the acidic conditions led to the desorption of $CaCO_3$ particles from the air–liquid interface resulting in the destabilization of the antibubbles and the release of drug-containing cores.

1. Introduction

When one or more liquid droplets are wrapped by a film of air in a bulk liquid, the resulting water-in-air-in-water ($W_1/A/W_2$) structure is referred to as an antibubble [1]. Similar to other related objects, such as emulsion droplets and foam bubbles, the antibubbles also require an

* Corresponding authors.
E-mail addresses: akmal.nazir@uaeu.ac.ae (A. Nazir), C.F.vanNostrum@uu.nl (C.F. van Nostrum).

https://doi.org/10.1016/j.jcis.2023.09.007
Received 19 May 2023; Received in revised form 31 July 2023; Accepted 1 September 2023
Available online 3 September 2023

appropriate stabilization mechanism. Based on the stabilization mechanism, they can principally be categorized as surfactant-, or particle-stabilized antibubbles [2]. The formation through surfactant is usually a one-step process, e.g., when a falling drop entraps an air film while impacting a bulk liquid [3]; however, this yields antibubbles with an extremely short lifetime, ranging from a few seconds to few minutes [2]. The short lifetime of antibubbles is specifically assigned to surfactants at the interface not being able to provide a sufficient barrier against rupture of the gas film. Consequently, when the gas film thins under the influence of gravity the gas film will eventually rupture leading to collapse of the antibubbles [4]. The particles-stabilized antibubbles, first introduced by Poortinga [5], are an alternative to the surfactant-based antibubbles as the particles at the interface can provide a long-term stability through formation of a rigid shell around the gaseous phase that contains liquid core(s). We hypothesize that these rigid particle shell prevents the gas film from rupturing. However, indications exist that when these particles are made to desorb or dissolve the antibubble returns to its inherently unstable state and will quickly collapse [6]. This opens up the possibility of producing antibubbles with triggered release behavior. The resulting combination of little leakage of the encapsulated active together with the possibility of a quick and complete release in the presence of a trigger provides an interesting opportunity for controlled drug release.

Multiple recent investigations have been directed toward the use of antibubbles stabilized by colloidal particles [6,8,9]. These particle-stabilized antibubbles are produced via a multiple-step process, i.e., i) formation of a Pickering $W_1/O/W_2$ double emulsion using a volatile oil, while a hydrophilic solute such as maltodextrin is present in both water phases, ii) quick freezing and lyophilization of the double emulsion, and iii) rehydration of the maltodextrin to produce $W_1/A/W_2$ structure. The colloidal particles remain at the interface (similar to the parent double emulsion) and thus maintain the three-dimensional structure of the produced antibubbles [5]. This has finally paved the way to build a unique encapsulation system in which the air film constitutes an impermeable barrier for encapsulated compounds. The antibubbles as a drug delivery system can offer exceptional protection to the loaded material, for instance, through avoiding possible interactions between core and shell. Furthermore, they can carry multiple materials of different polarity, as hydrophilic drugs can be loaded in the core while hydrophobic drugs could be initially dissolved in the oil phase of the emulsion that could later get deposited on the interface (on evaporation of the volatile oil) of the antibubbles. In recent years, a few exciting applications of antibubbles have been reported. For instance, antibubbles were used for encapsulating probiotics to protect them against low pH of the stomach [9]. Interestingly, the antibubbles can also be visualized inside the living tissues using diagnostic ultrasound (due to the presence of air), and the encapsulated drug can be released and delivered using clinically translatable ultrasound [8]. Most of the previously reported investigations on Pickering antibubbles have used fumed silica nanoparticles for the preparation of the parent Pickering double emulsion. Silica nanoparticles are generally recognized as safe by the U.S. Food and Drug Administration in adequate amounts and have extensively been applied in various biomedical applications [10]. Although ultrasound-guided delivery has successfully been reported for silica-based antibubbles, further research is required to produce antibubbles that can deliver the drug in response to other external stimuli. One such recent example is the use of nanoparticles of poly(lactic acid) (PLA) or its copolymers with glycolic acid (PLGA) to produce thermo-responsive antibubbles [6].

In continuation of the ongoing efforts to produce antibubbles with triggered release behavior (other than ultrasounds), here we report the suitability of bio-based $CaCO_3$ particles to produce acid-responsive antibubbles. Some other inorganic bio-based particles, e.g., calcium phosphate, tri-calcium phosphate, and hydroxy apatite, have been used as Pickering stabilizers in the past [11]. We opted for $CaCO_3$ particles because of their availability, low cost, and acid-responsive properties [12]. However, the native $CaCO_3$ particles are not surface active and are hydrophilic by their high surface energy [12,13]. There are two ways of surface modifications that can make $CaCO_3$ particles suitable for use as a Pickering emulsifier: i) ex-situ coating with suitable agents like soaps and surfactants [14,15] or ii) in-situ surface modification by using $CaCO_3$ particles along with a suitable surfactant, e.g., sodium dodecyl sulfate (SDS), or sodium stearoyl lactylate (SSL, which is a food-grade surfactant) [16]. Therefore, in the present study, we prepared two variants of $CaCO_3$-stabilized antibubbles using two functionally active $CaCO_3$ particles prepared by above mentioned approaches: i) $CaCO_3$ particles pre-coated with stearic acid ($CaCO_3$-SA), and ii) native $CaCO_3$ particles in combination with SSL as a surfactant ($CaCO_3$-SSL). We analyzed the suitability of both particles for fabricating acid-responsive antibubbles. Moreover, their size, encapsulation efficiency, and their pH response were compared with classic antibubbles produced with hydrophobized fumed silica particles. The acid-triggered release was studied using methylene blue (MB) as a model drug.

2. Materials and methods

2.1. Materials

The hydrophobized fumed silica particles, AEROSIL® R972 and AEROSIL® R816, were kindly provided by Evonik (Germany). The native (uncoated) calcium carbonate ($CaCO_3$) particles (CALOFORT® U) and stearic acid (octadecanoic acid) coated $CaCO_3$ particles (both manufactured at Specialty Minerals, USA) were supplied by Keyser & Mackay (The Netherlands). Sodium stearoyl-2-lactylate (SSL, S0846) was supplied by Tokyo Chemical Industry (Japan). The cyclohexane (≥99.5%) was purchased from Honeywell (USA). The maltodextrin ((2R,3S,4R,5R)-2,3,4,5,6-pentahydroxyhexanal) having a dextrose equivalent value of 2, methylene blue ([7-(Dimethyl-amino)phenothiazin-3-ylidene]-dimethylazanium chloride), Tween® 20 (polyoxyethylene (20) sorbitan monolaurate), Certipur® buffer solutions pH 2 (citric acid/sodium hydroxide/hydrogen chloride), Certipur® buffer solutions pH 5 (citric acid/sodium hydroxide/hydrogen chloride), and phosphate buffer pH 7 (di-sodium hydrogen phosphate/potassium dihydrogen phosphate) were provided by Merck (Germany).

2.2. Characterization of particles used for the formation of antibubbles

The size distribution and zeta potential of $CaCO_3$ (uncoated and coated) and silica (AEROSIL® R972 and AEROSIL® R816) particles were analyzed using Microtrac MRB's NANOTRAC Wave II (Microtrac Retsch GmbH, Germany) dynamic light scattering analyzer. Water (refractive index: 1.33) was used as a dispersant for both $CaCO_3$ particles and AEROSIL® R816 silica particles. Because AEROSIL® R972 silica particles are hydrophobic in nature, the DLS measurement was carried out after dispersing them in *n*-hexadecane (refractive index: 1.43). All the samples were prepared at a particle concentration of 0.5% and dispersed by sonicating using Branson Digital Sonifier SFX 550 (Emerson, USA) at 50% power for 1 min. The 'irregular' shape was selected for all the particles while creating the instrument's SOP, with refractive indices of 1.68 and 1.5 for $CaCO_3$ and silica particles, respectively (the values were taken from the instrument database). A measurement cycle consisted of three runs (each of 15 s), and then the average values for size distribution and zeta potential were recorded.

2.3. Preparation of Pickering double emulsions

The formation of double emulsion ($W_1/O/W_2$) was carried out through a two-step homogenization process, as shown in Fig. 1. A primary emulsion (W_1/O) was prepared by dispersing 5 mL deionized water (containing 0.1% MB as a model drug, and 10% maltodextrin) in 15 mL cyclohexane (volatile oil) containing 2.5% R972 hydrophobized fumed silica particles. The homogenization of this primary emulsion was

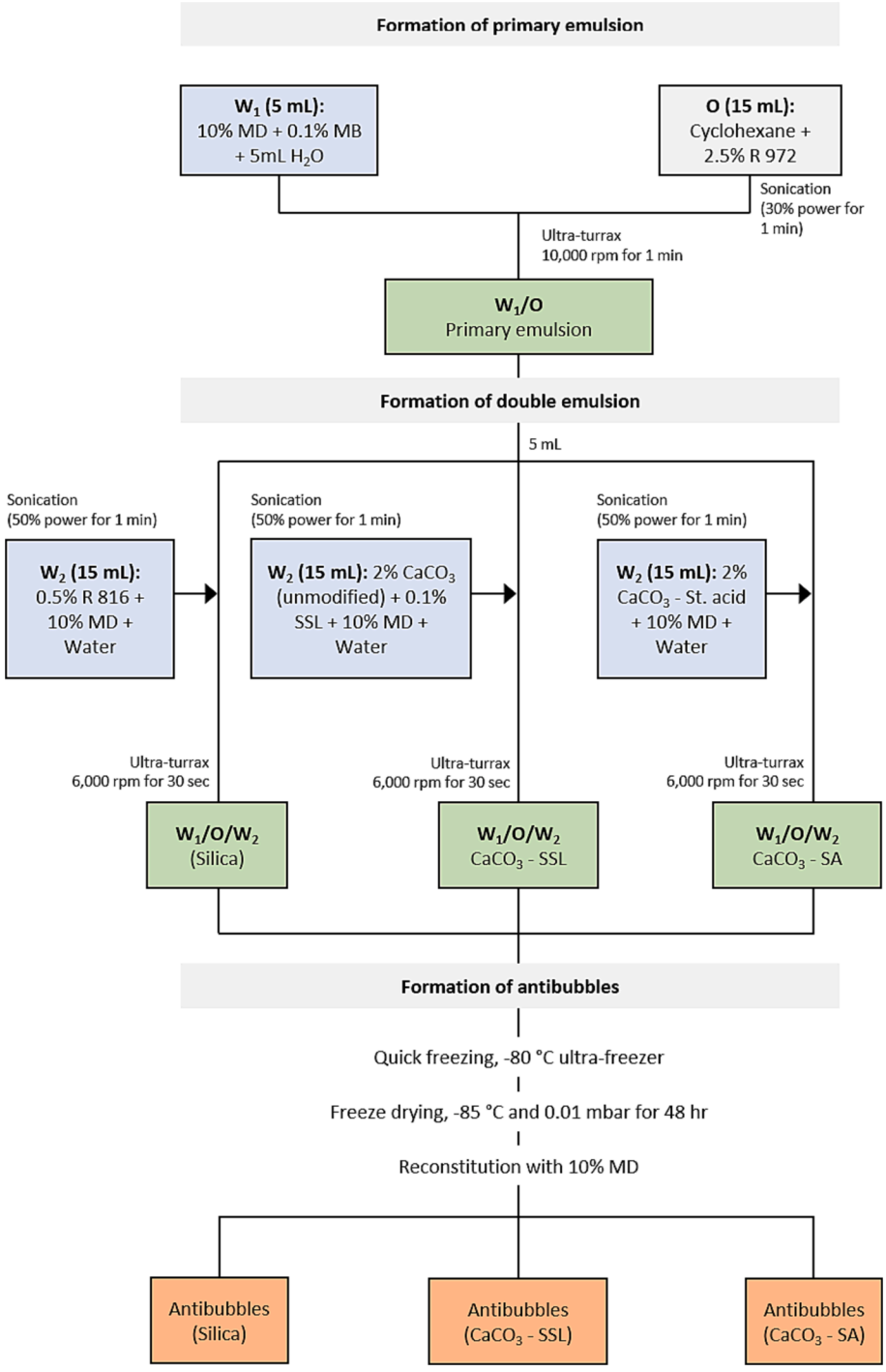

Fig. 1. A flow chart for the formation of different variants of antibubbles.

carried out in a 50 mL plastic tube using T25 digital ULTRA-TURRAX® (IKA, Germany) at 10,000 rpm for 1 min. Three different external water phases (W_2) were prepared containing 10% maltodextrin and various colloidal particles: i) R816 hydrophobized fumed silica particles (0.5%), ii) $CaCO_3$ unmodified particles (2%), and iii) stearic acid-coated $CaCO_3$ particles (2%). The mixture containing $CaCO_3$ unmodified particles was supplemented by SSL (0.1%). Before mixing with the rest of external water phase, SSL was dissolved by sonicating at 50% power for 3 min. All the colloidal particles in respective external water phases were dispersed by sonicating at 50% power for 1 min. Once all the external water phases were ready, the double emulsions were prepared by homogenizing 5 mL of previously prepared primary emulsion in 15 mL of W_2. The secondary emulsification step was carried out using T25 digital ULTRA-TURRAX® at 6,000 rpm for 30 *sec*.

2.4. Preparation of antibubbles

The produced double emulsions were quickly frozen in −80 °C ultra-freezer (BINDER GmbH, Germany). Afterwards, the frozen emulsion samples were lyophilized at −85 °C (0.01 mbar vacuum) using a freeze dryer (LyoAlfa 15, Telstar, Germany) for 48 h. Subsequently, the antibubbles (i.e., $W_1/A/W_2$) were produced by rehydration of the freeze-dried material with an aqueous maltodextrin solution.

2.5. Microscopic analysis

The parent double emulsions as well as antibubbles were observed under an optical microscope (Delphi-X observer, Euromax, The Netherlands) connected with a digital camera. A few drops of 10% maltodextrin were taken on a cavity glass slide and then one tiny drop of the emulsion was mixed and observed under the microscope. For observation of antibubbles, the lyophilized porous cake was carefully broken into smaller pieces with a needle making sure the sample was not crushed (that may deform the original microstructure). A small quantity of dried material (0.05 g) was rehydrated in 5 mL of the aqueous solution containing 10% maltodextrin. The mixture was kept for 5 min with some intermittent manual shaking to allow maximum rehydration of the material. Afterward, a drop of antibubble suspension was placed in a cavity glass slide and observed under the microscope. The images of all emulsion and antibubbles samples were recorded at 10X and 20X magnification powers of the microscope.

2.6. Scanning electron microscopy

The surface morphology of antibubble variants were examined in a scanning electron microscope, SEM (JSM-6010LA, JEOL, Japan), operated at an accelerating voltage of 15 keV. The freeze-dried material was manually sprinkled on the sample holder having a double-sided adhesive tape. All the samples were coated for 30 s (up to 3–5 nm thickness) with gold using a sputtering unit (Cressington Sputter Coater 108auto, Cressington Scientific Instruments, UK) to enhance the conductivity of the samples. Afterward, the samples were examined in SEM at different magnification powers and images were recorded.

2.7. Determination of size and polydispersity

The size of emulsion drops and antibubbles was recorded through image analysis of the optical microscopic images using ImageJ software [17]. For each measurement, the size of 100 emulsion droplets or antibubbles was measured (in triplicate), and then the average size (μ) and standard deviation (σ) were calculated. The polydispersity of emulsion drops and antibubbles was assessed through polydispersity index (PDI) as follows:

$$\mathrm{PDI} = \left(\frac{\sigma}{\mu}\right)^2 \tag{1}$$

2.8. Entrapment efficiency

The entrapment efficiency (EE) of double emulsions (immediately after formation) and antibubbles was indirectly measured from the concentration of MB that was released into the outer aqueous phase. In the case of double emulsion, 2 mL of a freshly prepared emulsion sample was taken in a microcentrifuge tube (Expell Secure, Germany) and centrifuged (MiPC 12, MiLab, UAE) at 1000 rpm for 1 min. The clear solution in the middle of each centrifuge tube was carefully drawn with the help of 10 mL sterile syringe, avoiding the creamed top layer. The liquid from the syringe was then poured into disposable plastic cuvette (Thermo scientific, UK) and the absorbance was taken in a UV spectrophotometer (Epoch 2 microplate spectrophotometer, BioTek, USA) at 665 nm for each sample. The MB concentration (mg/mL) (C_s) was quantified using a calibration curve obtained with known MB concentrations. The entrapment efficiency of each sample was calculated as follows:

$$\mathrm{EE}(\%) = \frac{C_{max} - C_s}{C_{max}} \times 100 \tag{2}$$

where, C_s and C_{max} represent the MB concentration in the sample and the maximum possible concentration (mg/mL) of methylene that can be released into the outer phase. The maximum possible release was obtained after adding Tween 20 into the same mixture used for the measurement of C_s (at a concentration of 10%). Principally, Tween 20 helps in the breakage of antibubble structure through change in wettability of the colloidal particles; hence, the encapsulated MB can be released into the external aqueous phase. For the determination of C_{max}, Tween 20-treated sample was centrifuged at 10000 rpm for 5 min and the absorbance was recorded at the same wavelength.

The encapsulation efficiency of antibubbles was measured as follows. A double emulsion sample (2 mL) was freeze-dried separately and then reconstituted to the same volume with water. The mixture was kept for 5 min with some intermittent manual shaking to allow maximum rehydration of the material. The rest of the procedure (i.e., to find C_s and C_{max}) was the same as already explained for emulsion samples.

2.9. Stability (release) of antibubbles at different pH

The stability of $CaCO_3$-SA and silica antibubbles at different pH was measured in terms of MB release from the cores. Buffer solutions of pH 2, pH 5 and pH 7 (5 mL each) were taken and maltodextrin was added in each buffer solution (at a concentration of 10%). This was followed by addition of 0.05 g of freeze-dried sample in each buffer solution and allowing to rehydrate for 2–3 min. An aliquot (2 mL) was drawn from each mixture and poured in a microcentrifuge tube, and then centrifuged at 2000 rpm for 2 min. The absorbance of the clear solution for each pH was taken in a spectrophotometer as explained above in Section 2.7. This absorbance value corresponds to the release of the drug at time 0. Similarly, the absorbance was recorded at 30, 60, and 90 min intervals. Finally, the samples were treated with Tween 20 to force the maximum release of MB from the antibubbles to determine the C_{max} (as explained in Section 2.7).

The cumulative release of MB from each antibubble variant was expressed as.

$$\text{Cumulative release}(\%) = \frac{C_s}{C_{max}} \times 100 \tag{3}$$

Furthermore, the release of $CaCO_3$-SA antibubbles was also monitored (using the same procedure) in a slightly buffered pH 7 solution (5 mL of water added to 5 mL pH 7 buffer) at 0 and 1.5 h. After 2 h, 10 mL of pH 2 buffer was added in the above-mentioned mixture (to mimic transfer to the stomach), and then the release of MB was measured again. Afterward, the mixture was treated with Tween 20 to record the release of complete drug from the cores (as explained in Section 2.7).

2.10. Data analysis

All the experiments were carried out in triplicate, and then the average and standard deviation of each data set were calculated using Microsoft Excel 2019 (Microsoft, USA). Subsequently, the data were presented graphically using GraphPad Prism 9 (GraphPad Software, Inc., USA).

3. Results and discussions

3.1. Characterization of silica and $CaCO_3$ particles used for the preparation of Pickering double emulsions

The size distribution of silica and $CaCO_3$ particles used for the preparation of Pickering double emulsions are shown in Fig. 2. The median diameter of both silica particles, i.e., AEROSIL® R972 and AEROSIL® R816, were around 0.2 μm, having a narrow size distribution. The uncoated $CaCO_3$ particles gave a bimodal distribution, having a peak in the nanoscale (median diameter around 600 nm) and another (comparatively smaller) peak in the microscale (median diameter 3 μm). The SA-coated $CaCO_3$ particles showed a single broader peak with a median diameter of 1.5 μm. As mentioned in Section 2.3, AEROSIL®

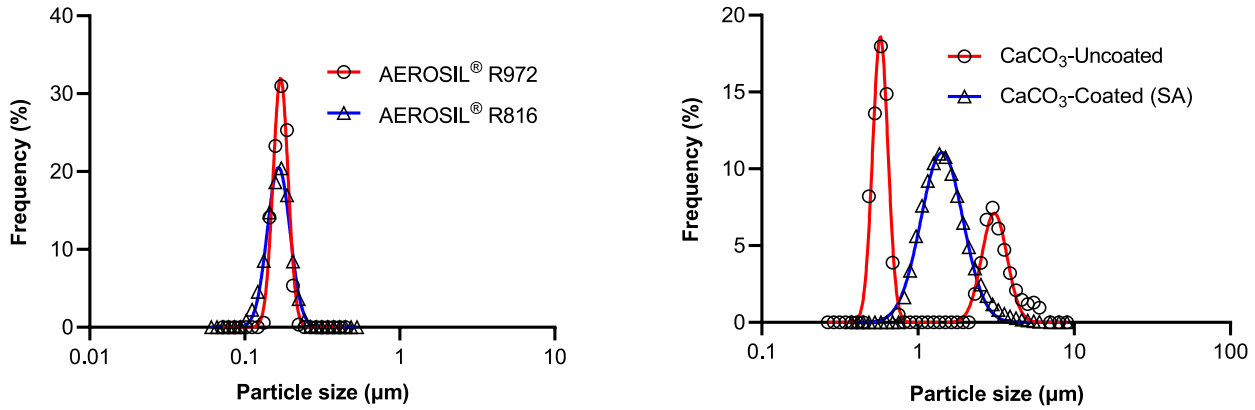

Fig. 2. The size distribution of silica and $CaCO_3$ particles used for the preparation of Pickering double emulsions.

R972 hydrophobic silica particles were used to stabilize the inner cores of all the three variants of double emulsions (antibubbles), i.e., the three formulation variants varied only for the type of particles added to the external water phase. Therefore, for a better understanding of the formulations, we measured the zeta potentials of AEROSIL® R816 and uncoated and SA-coated $CaCO_3$-particles. The zeta potential of AEROSIL® R816 was found to be −19.3 mV (close to the value reported by Dalvand et al. [18]), whereas uncoated and coated $CaCO_3$-particles displayed zeta potentials of + 23.8 mV and −35.6 mV, respectively, which are in accordance to previous studies [15,19,20]. A negative surface charge on coated $CaCO_3$ could be assigned to bi-layer formation of fatty acids on the $CaCO_3$ surface. In this arrangement there is a tail-to-tail interaction of stearic acid molecules, hence exposing the negative head groups of SA to the aqueous solutions leading to a more negative surface charge. Therefore, the surface charge changed here from positive 23.8 mV in case of uncoated $CaCO_3$ to negative 35.6 mV due to addition of stearic acid double layer to $CaCO_3$.

3.2. Characterization of antibubbles

The microscopic images of double emulsion and antibubble variants are shown in Fig. 3. Silica and $CaCO_3$-SA emulsion droplets as well as the corresponding antibubbles were more spherical in shape, as compared to $CaCO_3$-SSL emulsion droplets and antibubbles that appeared more pear-shaped or elongated. The formation of non-spherical shaped droplets is possible in case of Pickering emulsions, which usually occurs due to 'interfacial jamming' of particles [21,22]. The abundance of particles at the limited interfacial area causes interface to expand, and deform the droplet structure. At this point the motion of the particles is arrested because of the affinity of hydrophobic particles with each other resulting in a disordered shape instead of conventional spherical droplets. This effect is stronger for the more hydrophobic particles ($CaCO_3$-SSL in this case) because they have a stronger attractive interaction between each other. The antibubbles appear darker as compared to the parent double emulsion (Fig. 3). The dark color outside the cores in the antibubbles indicates the presence of air, as light is more strongly scattered by the air layer owing to a higher difference between the refractive index of air and that of the surrounding liquid. During the process of rehydration, the inner cores containing hygroscopic maltodextrin gain water through the diffusion of water vapor. The resulting hydrated cores are separated from the outer aqueous phase via a distinct air gap, as already established by Poortinga [5].

Fig. 4a shows SEM images of the three variants of antibubbles. Some cracked or broken antibubbles are pointed out that show the existence of multiple cores inside a single antibubble. It is assumed that at least the biggest particles are intact antibubbles with probably hidden cores inside. The insets of the three different antibubbles depict the surface morphology indicating that the silica antibubbles appeared relatively smoother compared to both $CaCO_3$ variants. A comparatively rough surface in case of $CaCO_3$ antibubbles could be due to a larger size of $CaCO_3$ particles (which also tend to aggregate) compared to the silica particles (as shown in Fig. 2).

The average size and polydispersity of all three variants of antibubbles are shown in Fig. 5. It can be observed that silica antibubbles have the smallest average size of 24 ± 2 μm, followed by the size of $CaCO_3$-SA antibubbles, i.e., 29 ± 3 μm. However, the antibubbles obtained from $CaCO_3$- SSL emulsion possess the largest mean diameter of 54 ± 5 μm and cover a broad range of 10–130 μm; around 50% of the antibubbles were of 50 μm and above, while for the other two antibubble variants majority of the antibubbles were less than 50 μm. The smallest size of the silica-stabilized antibubbles compared to the $CaCO_3$-stabilized antibubbles could be assigned to the silica particles possessing the smallest median size of 200 nm. The size distribution of $CaCO_3$-SA antibubbles was quite similar to the silica-based ones. That means that the $CaCO_3$-SA particles were surface active and sufficiently provided the interfacial stabilization to the antibubbles in spite of a relatively bigger median diameter than the AEROSIL® R816 silica particles.

Fig. 5d shows the entrapment efficiency of MB for the parent double emulsions and antibubbles. The entrapment efficiencies of emulsions and related antibubbles are comparable, which corroborates that the antibubble structure remained intact and can retain the encapsulated material. A non-significant difference was observed between the entrapment efficiencies of silica and $CaCO_3$-SA antibubbles, ranging from 80 to 85%. However, the entrapment efficiency of $CaCO_3$-SSL antibubbles was significantly lower than the other two variants, which was typically around 20%. The possible reasons behind a low entrapment efficiency of $CaCO_3$-SSL antibubbles are discussed in the next section.

3.3. Pre-requisites of antibubbles formation and the behavior of different particles at the interface

In this section, we will discuss some prerequisites for successful formation of antibubbles, which would help us to further understand the behavior of different particles used in this study. The antibubbles are composed of two interfaces i.e., inner W/A interface and outer A/W interface stabilized by adsorption of strongly hydrophobic and mildly hydrophobic particles at the interfaces, respectively. Indeed, the arrangement of particles at the interfaces of parent double emulsions is crucial in the formation of intact antibubbles. Any gap between the particles or a loose arrangement of the particles at the interface can alter or in severe cases destroy the structure of the emulsion during the freeze-drying. Therefore, a densely packed layer of particles at the interfaces determines the stability of resulting antibubbles. Here, it is also important to mention that the removal of the middle oil phase (during freeze-drying) favors the migration of more silica particles towards both

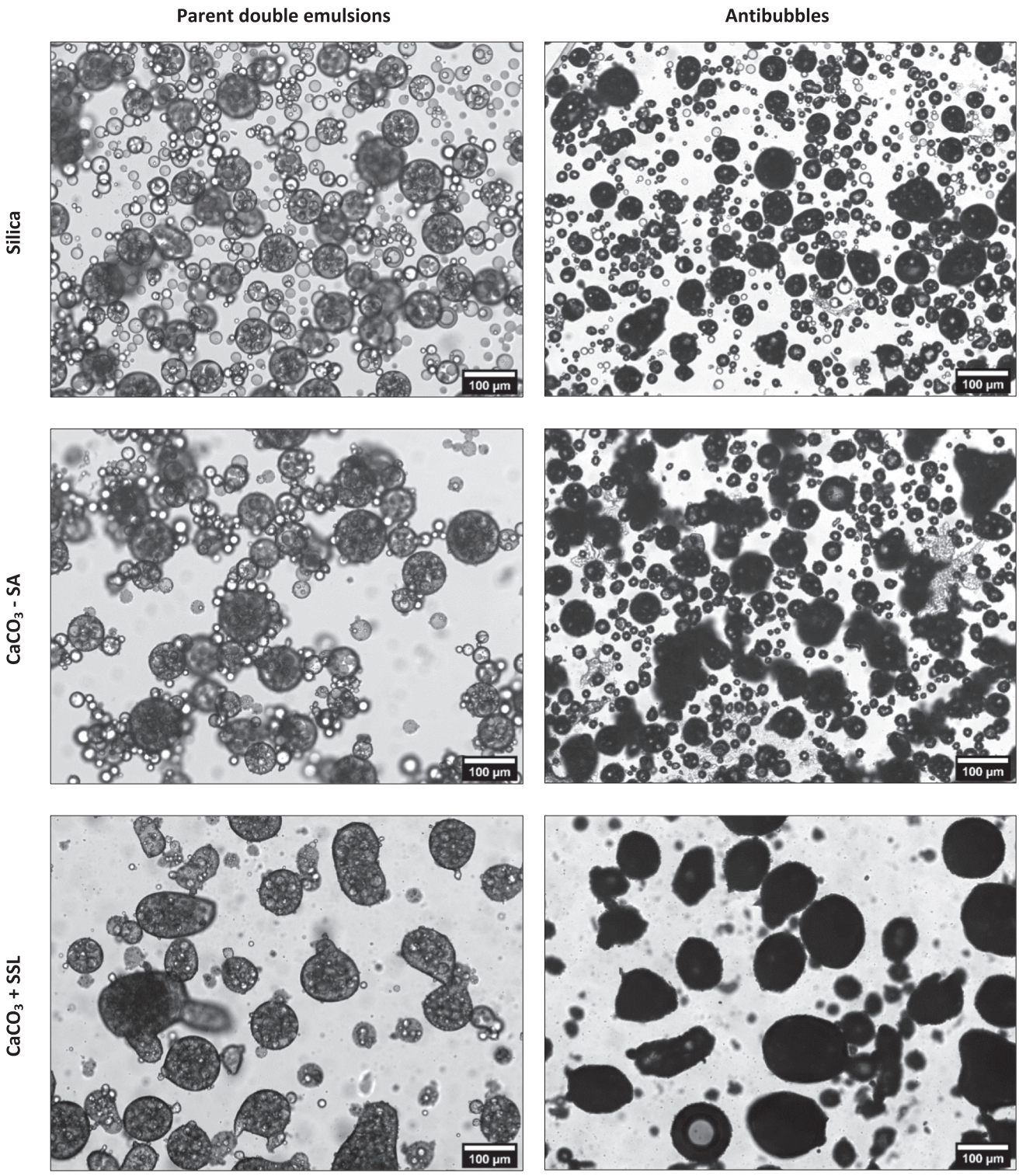

Fig. 3. Optical microscopic images of parent double emulsions and antibubbles.

interfaces. This was confirmed by Silpe et al. [23] who used Nile red coated silica particles in the oil phase. After analyzing the rehydrated antibubbles through confocal scanning laser microscopy, they observed a rather thick layer of aggregated silica particles at the interfaces. This could be similar to adsorption of particles on the interface from a volatile solvent in the form of Langmuir monolayers (in case of Pickering emulsions), with a difference that in case of antibubbles, the particles at the interface are more aggregated than simple monolayers [24]. Such densely packed layers of particles at the interface contribute to the integrity of the antibubbles during freeze-drying as well as when they are reconstituted. The strength of adhesion of the particles at the interface can be detected by the contact angle θ they make with the interface, which in turn relies on the wettability or affinity of the particles for two different fluids. The particles with extreme hydrophilicity ($\theta = 0°$) or hydrophobicity ($\theta = 180°$) are not suitable for attaching irreversibly at the interface; instead, particles with intermediate hydrophobicity are capable of irreversibly settling at the interface ($\theta = 90°$) [25]. In their native (uncoated) forms, both the particles that we

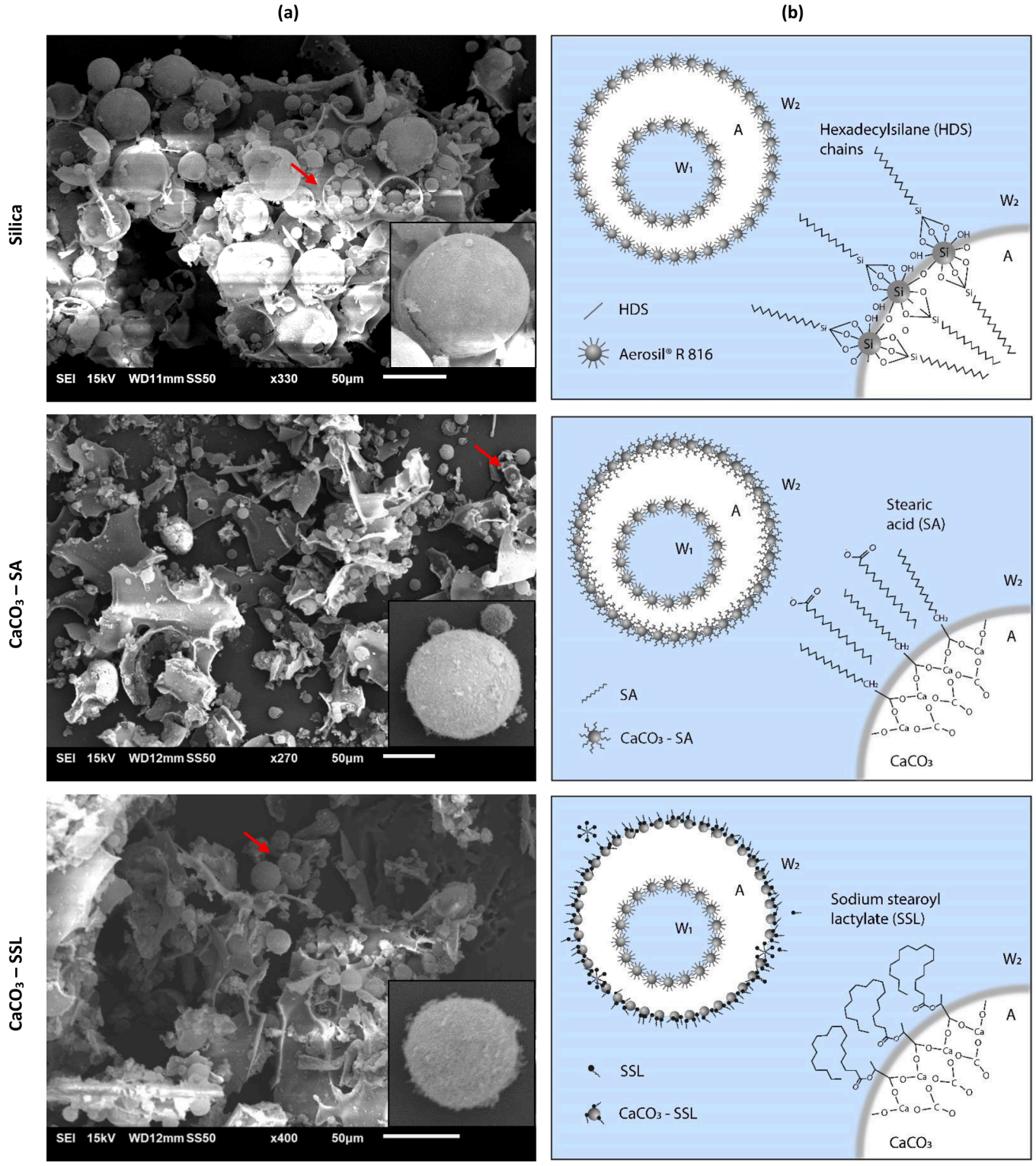

Fig. 4. A) the images of the freeze-dried mixture using scanning electron microscope (the red arrows show some broken antibubbles for different variants), and b) the schematic representation of the arrangement of particles at the interfaces of different antibubbles. (For interpretation of the references to color in this figure legend, the reader is referred to the web version of this article.)

used in our study, i.e., SiO_2 and $CaCO_3$, are hydrophilic in nature, and hence they are not capable of stabilizing Pickering emulsion. Therefore, in this study, silanized silica particles and modified $CaCO_3$ were used, as mentioned above.

For all the three antibubble variants, the inner core was stabilized with AEROSIL® R972 particles having a contact angle of around 110° at the water-cyclohexane interface [26]. Such hydrophobic particles are quite suitable for the preparation of a stable W/O primary emulsion [9]. Hence, the three antibubbles only varied for the outer A/W interface. Therefore, here we will only discuss the particles at the outer interface, which mainly control the integrity of the antibubbles in surrounding media. For the first variant, i.e., silica antibubbles, we used AEROSIL®

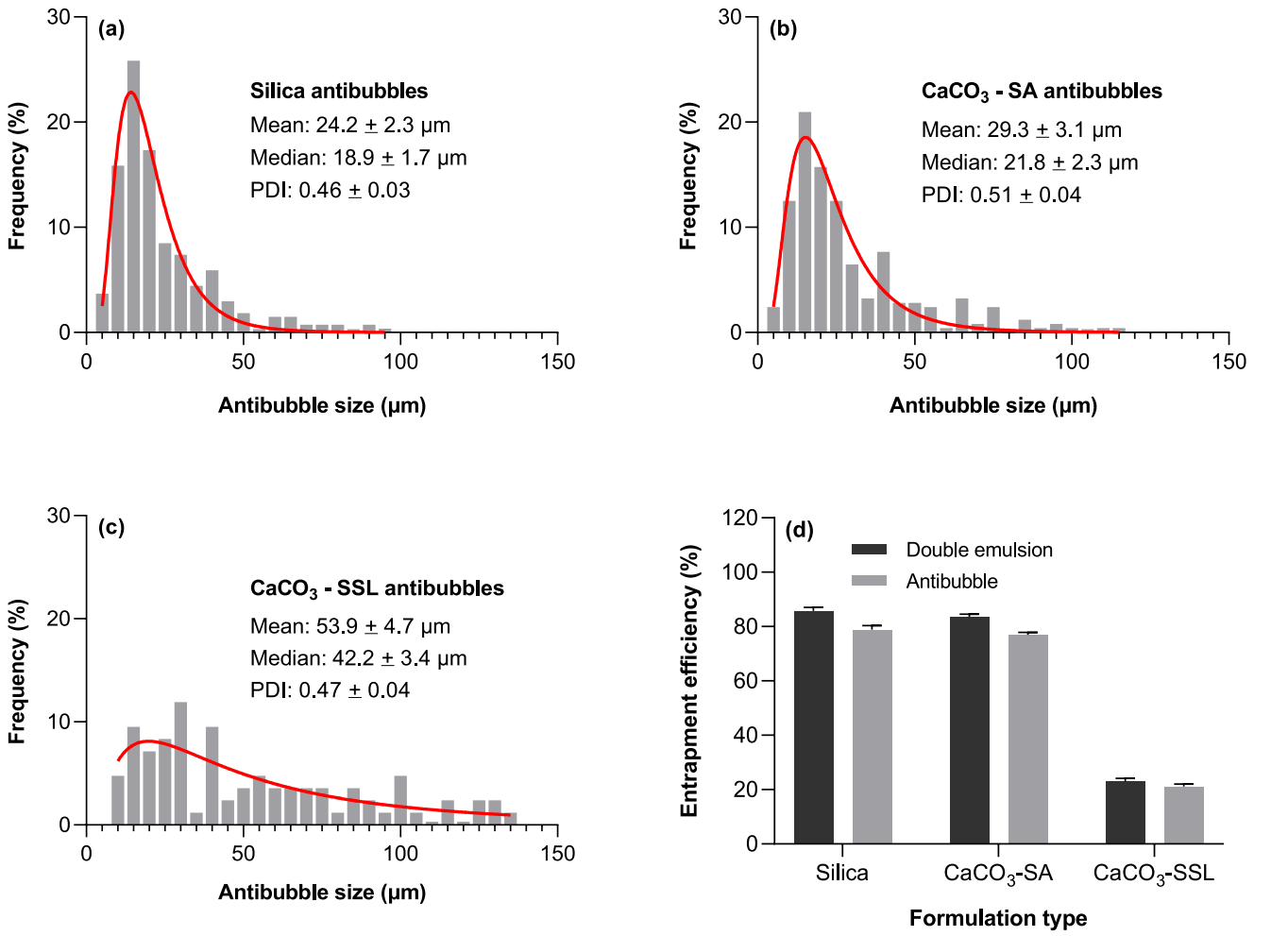

Fig. 5. The size distribution (a-c) and MB entrapment efficiency (d) of three antibubble variants: silica, $CaCO_3$-SA, and $CaCO_3$-SSL.

R816 at the outer interface. These particles are commercially made by carefully grafting hexadecyl silane equally on the surface of negatively charged hydrophilic silica. The particle surface has remaining –OH groups, which makes these silica particles intermediate hydrophilic/hydrophobic and allows energetically favorable adsorption at the O/W or A/W interface (Fig. 4b). For the second variant, we used $CaCO_3$ particles pre-coated with stearic acid. As a result of this chemisorption, polarity of the $CaCO_3$ particles is decreased, resulting in a better stability of the interface on particles adsorption (Fig. 4b). For the third variant, we tried in-situ hydrophobization of inorganic $CaCO_3$ particles using SSL, i.e. by chemisorption of SSL through its carboxylate ion to Ca^{2+} during formation of the emulsion [27,28]. However, the entrapment efficiency of MB by the $CaCO_3$-SSL based emulsion was significantly low as mentioned above. This indicates that $CaCO_3$-SSL particles were not very efficient in rapidly stabilizing the newly created interfaces during the second emulsification step, which has resulted in some leakage of the water phase from the inner cores. However, once the double emulsions have formed then they are stable enough to retain the cores during the subsequent processes leading to the formation of antibubbles (as indicated by same entrapment efficiencies of emulsions and corresponding antibubbles). There could be several reasons behind inefficiency of $CaCO_3$-SSL complex to provide complete stabilization of freshly prepared double emulsions. For instance, the surface properties of $CaCO_3$-SSL complex depend on the ratio between $CaCO_3$ and SSL, and how SLL molecules are distributed on the $CaCO_3$ particle surface. It has been shown by various studies, e.g., in Zhang et al. [29], that whenever an anionic surfactant is electrostatically attached with the $CaCO_3$ at a very low concentration, initially the particles remain hydrophilic. However, when the concentration of surfactant approaches its critical micelle concentration, the particles get fully occupied by the surfactant, and then the wettability of particles changes to become hydrophobic. On further increasing the concentration, the surfactants form a bilayer on the $CaCO_3$ particles surface with hydrophilic heads directing outwards, which makes particles again hydrophilic. So, a double phase inversion from an O/W emulsion into a W/O emulsion, and finally back into an O/W emulsion can be observed with change in surfactant concentration. This shows that SSL concentration is one of the critical factors in successful formation of double emulsions. Then another major reason could be that excess of surfactants in the free form or in form of micelles can compete with the $CaCO_3$-SSL composites at the interface as the free surfactants possess a higher migration speed, they tend to deposit on the interface quicker than $CaCO_3$-SSL [15,29]. As a result, the micelles or free surfactants cannot provide irreversible adsorption on the interface as in case of the particle or Pickering stabilization, with the risk of the leakage of inner cores resulting in low entrapment efficiency. Based on the above-mentioned factors we believe that a prudent regulation of surfactant is required for in-situ interfacial activation of particles. Furthermore, as this is a physical adsorption, therefore, a slight fluctuation of the surfactant concentration in the media can trigger desorption of SSL from the particle surface. Overall, our conclusion is that $CaCO_3$ pre-coated with SA is preferred compared to in situ SSL-coated particles.

3.4. Release behavior of silica and $CaCO_3$ antibubbles as function of pH and time

Given the low entrapment efficiency of $CaCO_3$-SSL antibubbles, our subsequent focus was exclusively on studying the release behavior of silica and $CaCO_3$-SA-based antibubbles. Fig. 6a depicts MB release from silica and $CaCO_3$-SA antibubbles immediately after 2–3 min of rehydration of respective freeze-dried powder at pH 2, 5, and 7. Besides assessing the initial release, we also measured the MB release as a function of time at each pH (Fig. 6 b-d). There was an instantaneous release of 18–24% of MB from silica antibubbles, which did not seem to be related to pH, nor was a continuous release observed for a prolonged period of time at any pH. On the contrary, $CaCO_3$-SA showed a high burst release (~60%) at pH 2, whereas the release at pH 5 and 7 was not significantly different from the instantaneous release from the silica antibubbles (Fig. 6a). This instantaneous release can probably be explained by non-encapsulated MB. Under acidic pH conditions, the cumulative release for the $CaCO_3$-SA antibubbles exhibited a rapid surge, reaching approximately 80% within 30 min after the initial burst release. In contrast, at neutral pH, the MB release from $CaCO_3$-SA was consistently below 40%.

The results presented in Fig. 6 showed that silica antibubbles were stable, even at low pH. This is due to a tight arrangement of silica particles at the interface, forming a rigid shell around the inner cores. The stability of silica-based antibubbles and protection of the payload under acidic conditions was also recently reported by Ghahfarokhi et al. [9], which was assessed through stability of encapsulated probiotics at pH 2 compared to the unencapsulated ones. The present study further confirms this through retaining a model drug in silica-based antibubbles at the different pH values. To understand the behavior of $CaCO_3$-SA antibubbles in acidic media, we need to consider the properties imparted to $CaCO_3$ particles by stearic acid. It is well known that the reaction between $CaCO_3$ and stearic acid gives calcium monostearate [30]:

$$\underbrace{CH_3(CH_2)_{16}COOH + CaCO_3}_{(Stearic\ \ acid)} \rightarrow \underbrace{CH_3(CH_2)_{16}COOCa^+ + HCO_3^-}_{(Ca-monostearate)} \quad (4)$$

$$CH_3(CH_2)_{16}COOCa^+ + H^+ \rightarrow CH_3(CH_2)_{16}COOH + Ca^{2+} \quad (5)$$

The carboxylate groups in calcium monostearate will be protonated at low pH. Once Ca^{2+} ions in calcium monostearate are replaced by H^+ ions (i.e., to form stearic acid again), the stearate is removed from the surface of $CaCO_3$, thus making them less surface active. As $CaCO_3$ particles alone are not surface active, hence are not capable of stabilizing interface, this could be the starting point for destabilization of $CaCO_3$-SA antibubbles at low pH, which further would lead to rapid dissolution of $CaCO_3$ releasing the core containing MB. Nonetheless, $CaCO_3$-SA antibubbles exhibited notable stability at neutral pH, similar to their silica-based counterparts.

The destabilization of $CaCO_3$-SA antibubbles under acidic conditions was also observed via an optical microscope. This was carried out through examining a drop of aqueous suspension (pH 7) of rehydrated $CaCO_3$-SA antibubbles on a glass slide under the microscope. The stable

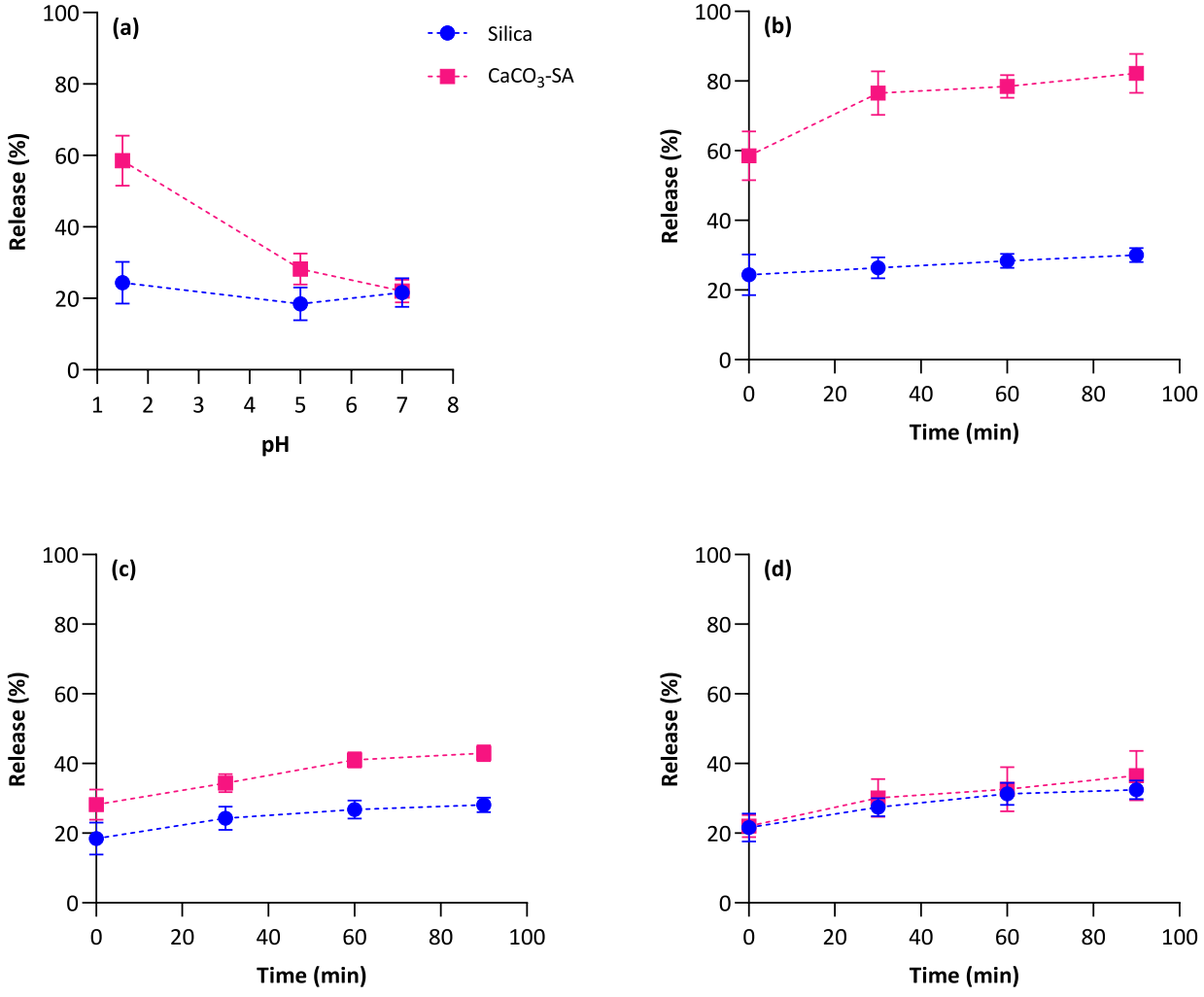

Fig. 6. The release behavior of silica and $CaCO_3$-SA antibubbles: (a) initial burst release at different pH, and release kinetics at (b) pH 2, (c) pH 5, and (d) pH 7.

antibubbles can be seen initially (Fig. 7), which usually appeared dark (as already discussed in Section 3.2). A rapid destabilization of $CaCO_3$-SA antibubbles was detected when a drop of 1 M HCl was added to the antibubble suspension (on the glass slide) resulting in the formation of bubbles, as indicated by some dotted squares in Fig. 7 (complete video can be seen in the supplementary material). These bubbles appeared spontaneously and then popped immediately. The formation of these bubbles could be due to: i) the release of CO_2 on interaction of acid with $CaCO_3$, and ii) the release of entrapped air from the antibubble structure (as the antibubble surface became distorted and cracked due to the added acid). Further, we expect that when the antibubble surface (i.e., the particle shell) is distorted, the cores are released into the external environment.

To further verify the acid-responsiveness of $CaCO_3$-SA antibubbles in actual conditions (i.e., transfer to the stomach), a freeze-dried sample was reconstituted with slightly buffered water of neutral pH and release was monitored for extended time of two hours. Then the pH was lowered with a buffer of pH 2 and release was taken again. This was done to make sure that the antibubbles do not rupture during the dissolution with water or in the oral cavity and only release the drug in the gastric conditions (i.e., upon arriving in the stomach). Fig. 8 depicts the release profile for this confirmatory experiment, which shows that the initial release (at neutral pH) was little above 20%, and moreover, it did not increase significantly in the same medium for the next one and half hour. However, as soon as the pH was lowered to 2, a burst release of around 80% was seen indicating a significant effect of low pH on $CaCO_3$-SA antibubbles (even higher than the burst release shown in Fig. 6b, which might be due a much longer rehydration time before lowering of the pH to 2). These results further augment the above-mentioned results, demonstrating that $CaCO_3$-SA could be a reliable candidate for gastric delivery of drugs.

The above shows that the gas shell of antibubbles acts as a good barrier to encapsulate actives and also can be made to burst in response to a trigger (acid) leading to quick release of the active. Use of gas as an encapsulant has recently been shown as well by other authors through closing of microchambers, also leading to little leakage in the absence of the release trigger and a quick and almost complete release in the presence of the trigger [7,31]. The low ratio between the rate of leakage of encapsulated active in the absence of a trigger and immediate release of the active in the presence of a trigger that we find here distinguishes our technology from previously reported triggered release systems [32].

4. Conclusions

In continuation to on-going efforts to produce stimuli-responsive antibubbles [6,8], acid-responsive antibubbles were produced for the first time using $CaCO_3$ particles pre-coated with stearic acid (SA) or by in situ coating with sodium stearoyl lactylate (SSL). Antibubbles with a

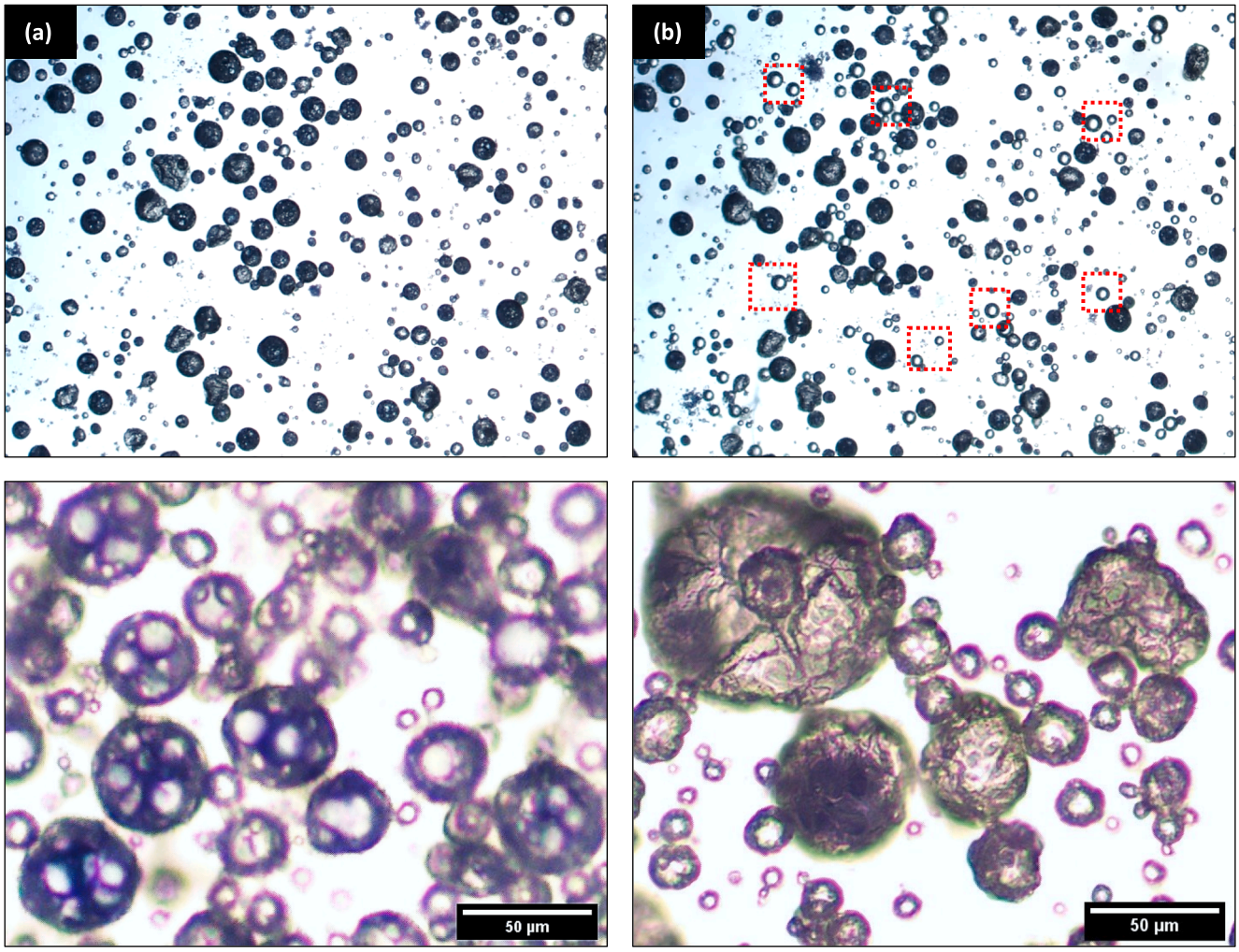

Fig. 7. The destabilization of CaCO3-SA antibubbles observed via an optical microscope after the addition of 1 M HCl. The images (a) and (b) are before and immediately after the addition of acid, respectively. The dotted squares represent the formation of bubbles immediately after the addition of acid. The bottom images are zoomed-in images of the top images, respectively.

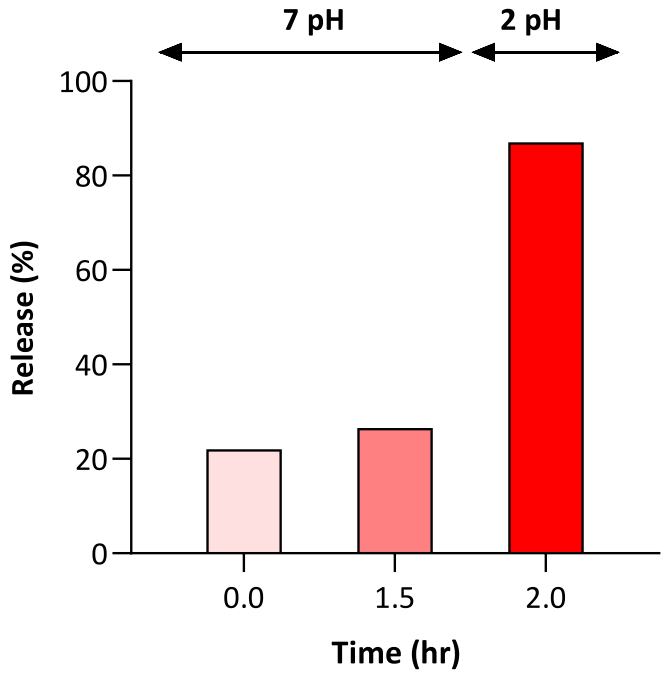

Fig. 8. The cumulative release of methylene blue from antibubbles after rehydration at pH 7 for a duration of 2 h. The pH of the antibubble suspension was lowered to 2 after 2 h.

high entrapment efficiency were obtained when they were stabilized by $CaCO_3$-SA particles. These antibubbles were extremely sensitive to an acidic medium, providing a significant burst release of the model drug (i.e., methylene blue) at pH 2. The entrapment of an air layer within these antibubbles acting as a release barrier, similar to previously reported antibubbles stabilized by silica particles [5,8,9,23], was confirmed through release of air bubbles when the antibubbles were exposed to 1 M HCl. The present study is an evidence that the $CaCO_3$-SA antibubbles can be used for gastric delivery of drugs, allowing high entrapment efficiency and a burst release of the encapsulated drug at gastric pH, which is usually an ideal release profile for targeted delivery [32]. Therefore, based on these findings, we consider loading of drugs in $CaCO_3$-SA antibubbles that require a gastric release (e.g., phenobarbital and secobarbital), especially in pediatric oral formulations to mask the bad taste of medicines.

CRediT authorship contribution statement

Rabia Zia: Investigation, Methodology, Formal analysis, Writing – original draft. **Albert T. Poortinga:** Conceptualization, Methodology, Resources, Supervision. **Akmal Nazir:** Methodology, Writing – review & editing, Funding acquisition. **Mutamed Ayyash:** Writing – review & editing, Resources. **Cornelus F. van Nostrum:** Writing – review & editing, Supervision, Project administration.

Declaration of Competing Interest

The authors declare that they have no known competing financial interests or personal relationships that could have appeared to influence the work reported in this paper.

Data availability

Data will be made available on request.

Acknowledgments

This study was supported by United Arab Emirates University (Grant no. 31F143) and Bether Encapsulate (The Netherlands).

Appendix A. Supplementary data

Supplementary data to this article can be found online at https://doi.org/10.1016/j.jcis.2023.09.007.

References

[1] Y. Vitry, S. Dorbolo, J. Vermant, B. Scheid, Controlling the lifetime of antibubbles, Adv. Colloid Interface Sci. 270 (2019) 73–86, https://doi.org/10.1016/j.cis.2019.05.007.
[2] R. Zia, A. Nazir, A.T. Poortinga, C.F. van Nostrum, Advances in antibubble formation and potential applications, Adv. Colloid Interface Sci. 305 (2022), 102688, https://doi.org/10.1016/J.CIS.2022.102688.
[3] P.G. Kim, H.A. Stone, Dynamics of the formation of antibubbles, Epl. 83 (5) (2008) 54001.
[4] D.N. Sob'Yanin,, Theory of the antibubble collapse, Phys. Rev. Lett. 114 (2015) 1–5, https://doi.org/10.1103/PhysRevLett.114.104501.
[5] A.T. Poortinga, Micron-sized antibubbles with tunable stability, Colloids Surfaces A Physicochem. Eng. Asp. 419 (2013) 15–20, https://doi.org/10.1016/j.colsurfa.2012.11.040.
[6] R. Araya-Hermosilla, F. Dervillé, N. Cohn-Inostroza, F. Picchioni, P.P. Pescarmona, A. Poortinga, Pickering Emulsions and Antibubbles Stabilized by PLA/PLGA Nanoparticles, Langmuir. 38 (2022) 182–190, https://doi.org/10.1021/ACS.LANGMUIR.1C02320/SUPPL_FILE/LA1C02320_SI_002.AVI.
[7] M. Gai, J. Frueh, T. Tao, A.V. Petrov, V.V. Petrov, E.V. Shesterikov, S. I. Tverdokhlebov, G.B. Sukhorukov, Polylactic acid nano- and microchamber arrays for encapsulation of small hydrophilic molecules featuring drug release via high intensity focused ultrasound, Nanoscale. 9 (2017) 7063–7070, https://doi.org/10.1039/C7NR01841J.
[8] S. Kotopoulis, C. Lam, R. Haugse, S. Snipstad, E. Murvold, T. Jouleh, S. Berg, R. Hansen, M. Popa, E. Mc Cormack, O.H. Gilja, A. Poortinga, Formulation and characterisation of drug-loaded antibubbles for image-guided and ultrasound-triggered drug delivery, Ultrason. Sonochem. 85 (2022), 105986, https://doi.org/10.1016/J.ULTSONCH.2022.105986.
[9] V. Mardani Ghahfarokhi, P.P. Pescarmona, G.-J.-W. Euverink, A.T. Poortinga, Encapsulation of lactobacillus casei (ATCC 393) by pickering-stabilized antibubbles as a new method to protect bacteria against low pH, Colloids and Interfaces. 4 (2020) 40, https://doi.org/10.3390/colloids4030040.
[10] M.A. Downing, P.K. Jain, Mesoporous silica nanoparticles: synthesis, properties, and biomedical applications, Nanoparticles Biomed, Appl. Fundam. Concepts, Biol. Interact. Clin. Appl. (2020) 267–281, https://doi.org/10.1016/B978-0-12-816662-8.00016-3.
[11] Z. Dong, L. Feng, W. Zhu, X. Sun, M. Gao, H. Zhao, Y. Chao, Z. Liu, CaCO3 nanoparticles as an ultra-sensitive tumor-pH-responsive nanoplatform enabling real-time drug release monitoring and cancer combination therapy, Biomaterials. 110 (2016) 60–70, https://doi.org/10.1016/J.BIOMATERIALS.2016.09.025.
[12] X. Guo, X. Li, L. Chan, W. Huang, T. Chen, Edible CaCO3 nanoparticles stabilized Pickering emulsion as calcium-fortified formulation, J. Nanobiotechnology. 19 (2021) 1–16, https://doi.org/10.1186/s12951-021-00807-6.
[13] Z.G. Cui, Y.Z. Cui, C.F. Cui, Z. Chen, B.P. Binks, Aqueous foams stabilized by in situ surface activation of CaCO3 nanoparticles via adsorption of anionic surfactant, Langmuir. 26 (2010) 12567–12574, https://doi.org/10.1021/LA1016559/SUPPL_FILE/LA1016559_SI_001.PDF.
[14] M. Suleymani, C. Ghotbi, S. Ashoori, J. Moghadasi, R. Kharrat, Theoretical and experimental study of foam stability mechanism by nanoparticles: Interfacial, bulk, and porous media behavior, J. Mol. Liq. 304 (2020), 112739, https://doi.org/10.1016/J.MOLLIQ.2020.112739.
[15] R. Zhang, L. Yang, R. Tu, J. Huo, J. Wang, J. Zhou, D. Chen, Emulsion phase inversion from oil-in-water (1) to water-in-oil to oil-in-water (2) induced by in situ surface activation of CaCO3 nanoparticles via adsorption of sodium stearate, Colloids Surfaces A Physicochem. Eng. Asp. 477 (2015) 55–62, https://doi.org/10.1016/j.colsurfa.2015.03.043.
[16] B.P. Binks, K. Muijlwijk, H. Koman, A.T. Poortinga, Food-grade Pickering stabilisation of foams by in situ hydrophobisation of calcium carbonate particles, Food Hydrocoll. 63 (2017) 585–592, https://doi.org/10.1016/j.foodhyd.2016.10.002.
[17] C.A. Schneider, W.S. Rasband, K.W. Eliceiri, NIH Image to ImageJ: 25 years of image analysis, Nat. Methods. 9 (2012) 671–675, https://doi.org/10.1038/nmeth.2089.
[18] A. Dalvand, S. Asleshirin, M. Fallahiyekta, Hydrophobic silica nanoparticle and anionic/cationic surfactants interplays tailored interfacial properties for the wettability alteration and EOR applications, Iran. J. Chem. Chem. Eng. 41 (2022) 1076–1094, https://doi.org/10.30492/IJCCE.2021.128675.4184.
[19] Z.G. Cui, C.F. Cui, Y. Zhu, B.P. Binks, Multiple phase inversion of emulsions stabilized by in situ surface activation of CaCO 3 nanoparticles via adsorption of fatty acids, Langmuir. 28 (2012) 314–320, https://doi.org/10.1021/la204021v.

[20] I. Ozen, S. Simsek, F. Eren, Production and characterization of polyethylene/calcium carbonate composite materials by using calcium carbonate dry and wet coated with different fatty acids, Polym. Polym. Compos. 21 (2013) 183–188, https://doi.org/10.1177/096739111302100310.
[21] E. Dickinson, Food emulsions and foams: Stabilization by particles, Curr. Opin. Colloid Interface Sci. 15 (2010) 40–49, https://doi.org/10.1016/j.cocis.2009.11.001.
[22] S.A.F. Bon, S.D. Mookhoek, P.J. Colver, H.R. Fischer, S. van der Zwaag, Route to stable non-spherical emulsion droplets, Eur. Polym. J. 43 (2007) 4839–4842, https://doi.org/10.1016/j.eurpolymj.2007.09.001.
[23] J.E. Silpe, J.K. Nunes, A.T. Poortinga, H.A. Stone, Generation of antibubbles from core-shell double emulsion templates produced by microfluidics, Langmuir. 29 (2013) 8782–8787, https://doi.org/10.1021/la4009015.
[24] V. Garbin, J.C. Crocker, K.J. Stebe, Nanoparticles at fluid interfaces: Exploiting capping ligands to control adsorption, stability and dynamics, J. Colloid Interface Sci. 387 (2012) 1–11, https://doi.org/10.1016/J.JCIS.2012.07.047.
[25] Z. Briceño-Ahumada, J.F.A. Soltero-Martínez, R. Castillo, Aqueous foams and emulsions stabilized by mixtures of silica nanoparticles and surfactants: A state-of-the-art review, Chem. Eng. J. Adv. 7 (2021), 100116, https://doi.org/10.1016/J.CEJA.2021.100116.
[26] J. Xie, D. Xue, D. Bao, X. Zhu, Y. Shao, H. Zhang, H. Zhang, J. Zhu, Enhanced flowability and film properties of ultrafine powder coatings modulated by modified flow additive, Prog. Org. Coatings. 179 (2023), 107483, https://doi.org/10.1016/j.porgcoat.2023.107483.
[27] M.C. Ortiz-Tafoya, A. Tecante, Physicochemical characterization of sodium stearoyl lactylate (SSL), polyoxyethylene sorbitan monolaurate (Tween 20) and κ-carrageenan, Data Br. 19 (2018) 642–650, https://doi.org/10.1016/J.DIB.2018.05.064.
[28] D. Kurukji, R. Pichot, F. Spyropoulos, I.T. Norton, Interfacial behaviour of sodium stearoyllactylate (SSL) as an oil-in-water pickering emulsion stabiliser, J. Colloid Interface Sci. 409 (2013) 88–97, https://doi.org/10.1016/J.JCIS.2013.07.016.
[29] R. Zhang, J.-H. Huo, Z.-G. Peng, W.-J. Luo, Q. Feng, J.-X. Wang, J. Zhang, Study on the interaction of CaCO3 nanoparticles and surfactant in emulsion phase transition and its molecular dynamics simulation, Colloids Surfaces A Physicochem. Eng. Asp. 511 (2016) 105–112.
[30] Z. Cao, M. Daly, L. Clémence, L.M. Geever, I. Major, C.L. Higginbotham, D. M. Devine, Chemical surface modification of calcium carbonate particles with stearic acid using different treating methods, Appl. Surf. Sci. 378 (2016) 320–329, https://doi.org/10.1016/j.apsusc.2016.03.205.
[31] M. Gai, J. Frueh, V.L. Kudryavtseva, A.M. Yashchenok, G.B. Sukhorukov, Polylactic acid sealed polyelectrolyte multilayer microchambers for entrapment of salts and small hydrophilic molecules precipitates, ACS Appl. Mater. Interfaces. 9 (2017) 16536–16545, https://doi.org/10.1021/acsami.7b03451.
[32] M. Liu, X. Wang, Y. Wang, Z. Jiang, Controlled stimulation-burst targeted release by pH-sensitive HPMCAS/theophylline composite nanofibers fabricated through electrospinning, J. Appl. Polym. Sci. 137 (2020) 48383, https://doi.org/10.1002/app.48383.